



# Unraveling the molecular dynamics of wound healing: integrating spatially resolved lipidomics and temporally resolved proteomics

Hongxia Bai<sup>1</sup> · Alejandra Suarez Arnedo<sup>2</sup> · Yining Liu<sup>2</sup> · Tatiana Segura<sup>2</sup> · David Muddiman<sup>1</sup>

Received: 17 November 2024 / Revised: 20 February 2025 / Accepted: 12 March 2025 / Published online: 24 April 2025  
© The Author(s) 2025

## Abstract

Understanding the spatial–temporal molecular dynamics of wound healing is crucial for devising effective treatments. Three-dimensional mass spectrometry imaging (3D MSI) enables the comprehensive visualization of molecular distribution throughout skin layers, offering valuable insights into the wound healing process. However, traditional 3D MSI often faces challenges in maintaining data integrity and accurate image registration in the third dimension. To address this, we employed infrared matrix-assisted laser desorption electrospray ionization (IR-MALDESI), a hybrid ambient ionization technique capable of sequential imaging through consecutive ablation events for precise 3D image reconstruction. Herein, 3D IR-MALDESI MSI was used to compare the lipidome of fresh-frozen wound samples at three stages of wound healing (inflammation, proliferation, and remodeling) with the healthy skin of SKH-1 mice. Supplementing this data with a refined LC–MS-based proteomics protocol on selected wound biopsies, our integrated approach deepens our understanding of the molecular intricacies inherent in tissue regeneration.

**Keywords** Wound healing · Mass spectrometry imaging · 3D · IR-MALDESI · Multi-omics

## Introduction

As the body's most extensive organ, the skin provides a critical barrier against external threats such as pathogens and various stimuli. Its integrity, once disrupted by injury, must be promptly restored to preserve its protective function. The complex process of wound healing requires the concerted interplay of diverse cell types, including neutrophils and macrophages, and unfolds in three overlapping stages: inflammation, proliferation, and remodeling [1]. A disruption in this progression may culminate in chronic wounds, ulcers, or excessive scarring [2].

Chronic wounds afflict millions of people, particularly with a rising incidence of diabetes and aging population in the USA; subsequently, this propagates to a significant economic burden, exceeding \$25 billion annually for treatment

measure [3]. While recent advancements have shed light on certain aspects of wound healing, a comprehensive molecular understanding remains a challenge. Despite numerous research efforts to understand the overall patterns of proteins involved in wound healing [4–6], a comprehensive understanding of the interaction between proteins and other compounds such as lipids remains incomplete.

Mass spectrometry, particularly mass spectrometry imaging (MSI), is revolutionizing the approach to analytical challenges [7]. While MSI adeptly elucidates the spatial distribution of a variety of molecules in a single label-free experiment [8], it has a significant drawback: sampling bias from studying 3D biological events with 2D sections. The newer three-dimensional mass spectrometry imaging (3D MSI) is emerging as a method to capture more comprehensive sample data [9]. Traditional 3D mass spectrometry imaging (MSI) approaches often rely on serial sectioning to generate volumetric data, a process that can result in significant loss of biological information and challenges in achieving accurate 3D image reconstruction [10]. Alternatively, techniques leveraging continuous ablation beams, such as ion or laser beams, have been developed. These methods enable direct sampling of the sample's surface while simultaneously exposing fresh layers for subsequent imaging,

✉ David Muddiman  
demuddim@ncsu.edu

<sup>1</sup> Biological Imaging Laboratory for Disease and Exposure Research (BILDER), Department of Chemistry, North Carolina State University, Raleigh, NC 27695, USA

<sup>2</sup> Department of Biomedical Engineering, Duke University, Durham, NC 27708, USA

thereby bypassing the need for physical sectioning. Secondary ion mass spectrometry (SIMS) has been a pioneering approach in this domain, utilizing dynamic ion beams to facilitate high-resolution molecular depth profiling and 3D imaging of biological systems [9, 11, 12]. However, SIMS is often constrained by its small molecular ion generation and challenges in handling complex biological matrices. In contrast, infrared matrix-assisted laser desorption electrospray ionization (IR-MALDESI) facilitates 3D imaging with laser ablation, generation of a 3D molecular profile by continuously imaging the same region while ablating through the sample depth [13, 14]. Preliminary studies have validated IR-MALDESI's suitability for biological studies, demonstrating its efficacy on both over-the-counter pharmaceuticals (hard) and tissue samples (soft) without the need for tedious sample preparation [13, 14].

Understanding wound healing is intricate and requires a holistic multi-omics approach for comprehensive molecular assessment. Lipids, despite their quintessential role in skin function, have their spatial dynamics in wound healing underrepresented in the literature. Phospholipids, particularly glycerophospholipids and sphingolipids, have recently been reported as bioactive lipids essential for intra- and intercellular communication and maintaining cell membrane structure [15]. Eicosanoids, especially those from the cyclooxygenase (COX) pathway, are crucial in this context. They influence various stages of wound healing, from platelet aggregation to tissue remodeling, with molecules like thromboxane A2 (TxA2), prostaglandin E2 (PGE2), and prostaglandin D2 (PGD2) playing pivotal roles [16]. The significance of arachidonic acid and its metabolites (e.g., leukotrienes and prostaglandins) in maintaining balance and managing inflammation is undeniable [17]. Furthermore, recent research highlights the emergence of pro-resolving mediators like resolvins in response to wound stimuli, underscoring the evolving understanding of lipid-mediated wound healing [18]. Simultaneously, the use of proteomic techniques, drawing on tissue biopsies and wound exudates, has significantly enriched our knowledge of wound healing [19, 20]. These methods reveal potential therapeutic targets and markers for healing progression with a recurring focus on proteins like elastase, growth factors, fibronectin, and matrix metalloproteases such as MMP-2 and MMP-9 [19, 21].

Despite these independent endeavors into lipidomics and proteomics, integrative studies that combine these data remain sparse. Recent advancements in multi-omics approaches have demonstrated their ability to bridge this gap, offering a more comprehensive understanding of molecular dynamics. Studies integrating spatially resolved metabolomic and lipidomic data with proteomics have revealed cell-type-specific metabolic and lipidomic variations, highlighting tissue heterogeneity during physiological and pathological processes [22–24]. For instance, 3D mass

spectrometry imaging has illuminated the interplay between metabolic and lipid pathways in host–pathogen interactions [25], while large-scale efforts like the Human BioMolecular Atlas Program (HuBMAP) have underscored the importance of spatially resolved omics in mapping cellular diversity and molecular interactions [26]. These findings underscore the potential of integrated approaches in studying complex biological phenomena, including wound healing.

In this study, we investigated the process of wound healing using a full-excisional murine healing model with SKH-1 mice. We employed an integrative approach, combining 3D IR-MALDESI MSI for lipidomic analysis and bottom-up proteomics by LC–MS, to examine the different stages of wound healing. Through 3D MSI, we investigated lipid distribution, and proteomics allowed us to identify proteins potentially involved in wound healing. While this work offers preliminary molecular insights into the healing process, future studies with expanded datasets and additional biological replicates will be critical to fully validate these findings and translate them into therapeutic strategies for managing wounds.

## Experimental details

### Materials

In this study, an 11-week male SKH1 mouse model was purchased from Charles River Laboratories. Biopsy punch pens of various sizes used to create the wounds, were purchased from Integra Miltex. The following materials were sourced from Thermo Fisher Scientific (Wilmington, DE) and used for proteomic analysis: 1 M Tris–HCl solutions (pH 7.5 and 8.0), sodium chloride (NaCl), ammonium bicarbonate (ABC), Pierce™ trypsin protease (MS grade), LC/MS grade water (H<sub>2</sub>O), LC/MS grade acetonitrile (ACN), LC/MS grade formic acid (FA), Vivacon 500 30 kD MWCO filters, and the Pierce™ BCA Protein Assay Kit. Other reagents, such as urea, dithiothreitol (DTT), and iodoacetamide (IAA) were procured from Bio-Rad (Hercules, CA).

### Wound healing study

Male SKH-1 Elite mice (8–12 weeks old) were housed in a centralized animal facility at Duke University. We used an excisional splinted wound protocol as described in previous publications [27, 28]. The mice were anesthetized with 4% isoflurane (1.5–2% isoflurane for maintenance), injected with Buprenorphine SR (1 mg/mL, 0.5 µg per g of mouse weight) subcutaneously before surgery, and placed on a warming pad. Four clean, well-defined wounds were created along the middle of the animal's back using sterile 5 mm biopsy punches after the dorsal surface was sterilized

with iodine and ethanol. PDMS ring splints with a 7-mm wide window were adhered around the wounds to prevent contraction and allow for healing through re-epithelialization and granulation. Wounds were treated with clinically used standard treatment Woun'Dres [28]. Tegaderm dressings were applied to the back to prevent the wounds from drying out. The animals were weighed and checked every other day and housed individually in cages. All procedures were approved by the Duke University Institutional Animal Care and Use Committee and followed the NIH Guide for the Care and Use of Laboratory Animals.

### Experimental design and sample collection

Following wounding, the mice were kept for 4, 14, and 21 days before being euthanized using Carbon dioxide (CO<sub>2</sub>) inhalation and cervical dislocation. 7-mm biopsy punch samples of the wounded areas with adjacent tissue and samples of unwounded healthy skin were collected and immediately frozen in a bath with acetone and isopentane on foil-taped glass slides for lipidomic analysis.

Additionally, 1.5 mm biopsy punch samples were collected for proteomic analysis using low-binding 1.5 mL tubes. All samples were stored in a – 80 °C freezer until the mass spectrometry imaging measurements were conducted.

The detailed experimental workflow is illustrated in Fig. 1. Dermal excisional wound samples were obtained at three critical time periods: day 4, representing the inflammation phase; day 14 for the proliferation phase; and day 21, indicative of the regeneration phase [28]. Three samples were collected for day 4 and 14, four samples for day 21 and five samples of unwounded healthy skin. A subsequent biopsy of 1.5 mm was extracted from the epicenter of each wound. This biopsy underwent comprehensive proteomics sample processing, including tissue homogenization, protein extraction, and the filter-aided sample preparation (FASP) method, to obtain purified peptide samples for bottom-up proteomics analysis. The residual portion of each wound sample was subjected to an analysis via IR-MALDESI MSI, a technique specifically chosen for its ability to map and define the lipidome with spatial accuracy.

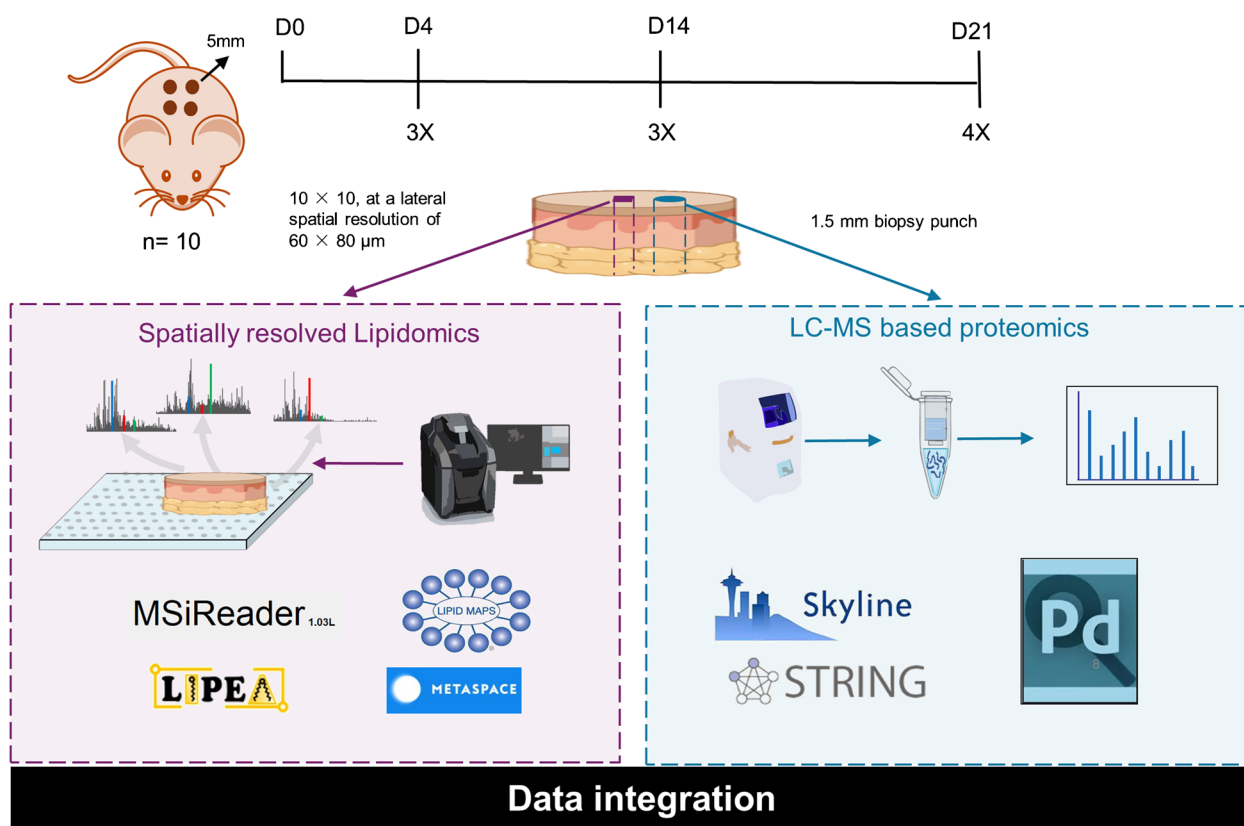


**Fig. 1** Overall workflow for wound healing experiments: Dermal excisional wounds were created using a 5-mm biopsy punch and harvested at specific time points (4, 14, and 21 days) to represent inflammation, proliferation, and regeneration stages. The number of replicates collected at each time point are specified. From each harvested sample, a 1.5 mm biopsy was taken from the wound center and pro-

cessed using a typical proteomics workflow involving homogenization, extraction, and FASP. The remaining wound sample underwent analysis using IR-MALDESI MSI to investigate the spatially resolved lipidome. Integration of the proteomics and lipidomic data provided insights into the wound healing process

## IR-MALDESI imaging platform

An in-house developed IR-MALDESI source was integrated with an Orbitrap Exploris 240 mass spectrometer (Thermo Fisher Scientific, Bremen, Germany) for imaging purposes [29]. The ion source employed water/ice matrix-assisted laser desorption, complemented by post-ionization through electrospray. An infrared laser (JGM Associates, Inc., Burlington, MA, USA) with an output energy between 0.4 and 0.5 mJ and a wavelength of 2.97  $\mu\text{m}$  was used to ablate the sample surface. The ablated material was then directed into an orthogonal electrospray plume, which was generated with a flow rate of a 1.5  $\mu\text{L}/\text{min}$  and a voltage of 3500 V. Mass spectra acquisition was performed in positive mode, ranging from  $m/z$  150–600. The system was operated with the EASY-IC enabled, automatic gain control (AGC) deactivated, and a mass resolving power set at 240,000<sub>FWHM</sub> at  $m/z$  200. For optimal synchronization with ion generation, an injection time of 25 ms, and a handshake delay time of 140 ms were utilized.

The imaging process was controlled by the custom software RastirZ [30]. Imaging was completed across 40 layers with a region of interest (ROI) of  $10 \times 10$ , at a lateral spatial resolution of  $60 \times 80 \mu\text{m}$ . To prevent the laser from losing focus during continuous ablation, manual stage adjustments were executed to ensure the laser remained within its depth of focus. After ablation, the sample craters' depth was gauged using a Keyence confocal microscope (VK-X1100, Keyence, Itasca, IL, USA). This measurement facilitated determining the necessary  $z$ -resolution adjustment to uphold the laser's focus.

## LC–MS based proteomics workflow

The LC–MS-based proteomics workflow began with the homogenization of a 1.5-mm biopsy, derived from the same sample as MSI, using a GenoGrinder (Spex Sample Prep, NJ, USA). Homogenization parameters included a force of 1400 g, alternating between 30-s grinding cycles and 30-s rest intervals, repeated for a total of four cycles. For optical protein solubility, three 2.9 mm diameter beads were used combined with 100  $\mu\text{L}$  of 50 mM ABC and 1% SDC. Following homogenization, protein concentrations were measured with a BCA assay, and an aliquot equivalent to 15  $\mu\text{g}$  of total protein was subject to a modified filter-aided sample preparation workflow [31, 32].

In brief, samples underwent reduction in 50 mM dithiothreitol with 0.1 M Tris–HCl (pH 8.0) at 56 °C for 30 min. Afterward, samples were placed onto a 30 k Da MWCO filter and centrifuged to remove surplus dithiothreitol. Next, alkylation was performed by treating the samples with 64  $\mu\text{L}$  of 200 mM iodoacetamide in 8 M urea in 0.1 M Tris–HCl pH 8.0 for 1 h at room temperature in the dark.

Excess iodoacetamide was eliminated via centrifugation, and retained proteins were thrice washed using 2 M urea, 10 mM calcium chloride in 0.1 M Tris–HCl (pH 8.0). This was followed by pH adjustment and purification using 0.1 M Tris–HCl (pH 7.5). The samples then underwent overnight digestion at 37 °C using 0.5  $\mu\text{g}$  of trypsin, resulting in tryptic peptides, which were stored at  $-20$  °C pending LC–MS/MS analysis.

The proteomics measurements were performed using a Thermo EASY nano LC 1200 interfaced with an Orbitrap Exploris 480 mass spectrometer (Thermo Fisher Scientific, Bremen, Germany). The setup employed a “trap-and-elute” configuration with specific column dimensions: a 0.075 mm  $\times$  20 mm C<sub>18</sub> trap column and a 0.075 mm  $\times$  250 mm C<sub>18</sub> analytical column. The analysis involved injecting 2  $\mu\text{L}$  of the sample peptides (1  $\mu\text{g}/\mu\text{L}$  in 2% acetonitrile in water with 0.1% formic acid) and maintaining a nanoLC flow rate of 300 nL/min. Elution of peptides was achieved using a 135-min gradient with varying concentrations of Mobile Phase B (MPB). The eluted peptides were ionized in the ion source with 1.9 kV applied, and data acquisition was performed using full MS scans and data-dependent acquisition (DDA) MS/MS. The other instrument settings included a scan range of 375 to 1600, a resolving power of 120,000<sub>FWHM</sub> (at  $m/z$  200), a 120 ms maximum injection time, an HCD normalized collision energy set at 30%, and dynamic exclusion intervals lasting 20 s periods.

## Data analysis

For MSI, the XCalibur raw data were converted to imzML format using an open-source *raw to imzML converter* software [33]. Once converted, the imzML files were subsequently analyzed using the MSiReader software (v1.03) for both data visualization and statistical analysis [34, 35]. The “Peakfinder” algorithm in this software was employed to identify unique ions based on two constraints. Firstly, a peak had to be present in more than 80% of the interrogated zone and present in less than 20% of the reference zone. Secondly, if a peak was present in more than 20% of the reference zone, the average abundance ratio (reference: interrogated) must exceed 2. This approach allowed for the identification and characterization of specific ions of interest in the MSI datasets.

Potential lipids were annotated at the formula level using LipidMaps [36], with a set mass accuracy constraint of  $\pm 2.5$  ppm. After this, the identified potential lipids underwent lipids pathway enrichment analysis using the LIPEA tool (<https://lipea.biotec.tu-dresden.de/home>). The primary aim of this analysis was the identification of significantly perturbed pathways in relation to the lipids detected, utilizing the Kyoto Encyclopedia of Genes and Genomes (KEGG) database. The Over-Representation (or enrichment) Analysis



(ORA) was employed to determine pathways that were over-represented compared to the background *Mus musculus* (*M. musculus*) lipids database. This comprehensive analysis provided insights into the functional pathways associated with the identified lipids in the study.

In the proteomics analysis, the raw data was searched against the *M. musculus* fasta database using Proteome Discoverer 2.5 (Thermo Scientific, San Jose, CA) with the SEQUEST HT algorithm. The search parameters included trypsin (full) as the digesting enzyme, allowing for a maximum of 3 missed trypsin cleavage sites, a precursor mass tolerance of 5 ppm, and a fragment mass tolerance of 0.02 Da. Peptide validation was performed using Percolator, with a *q*-value threshold set to achieve a minimal false discovery rate (FDR) of less than 0.01. Proteome Discoverer was also utilized to analyze differentially expressed proteins among different sample groups, generating label-free relative quantification data. Both unique and razor peptides were used for relative quantification, without any normalization or scaling applied. To test the hypothesis of fold change based on the summed protein abundance, an analysis of variance (ANOVA) test was performed. Classification, functional enrichment, and protein interaction analysis of the proteins were performed using STRING (v12). Expression analyses like Volcano plots, and Venn's diagram, were made using VolcanoNoseR [37], and InteractiVenn [38] respectively. Additional graphs were plotted using GraphPad Prism software 9 (GraphPad Software, San Diego, CA, USA).

## Results and discussion

Wound healing represents a multifaceted physiological response, marked by a dynamic interplay of cellular activities and molecular pathways [39]. To navigate this complexity, the present approach harnessed the capabilities of IR-MALDESI for lipidomic profiling and LC-MS/MS for proteomic analysis. Utilizing IR-MALDESI, the 3D resolved lipidomic configuration of mouse skin samples had been previously mapped, offering a detailed insights into the volumetric distributions of varied lipids [14]. Building on this established methodology, we applied IR-MALDESI to wounded skin specimens to explore lipidomic dynamics across different stages of wound healing. This approach offers a preliminary perspective on lipid behavior during the healing process and lays the foundation for further integrative studies.

### Depth resolution and system repeatability in IR-MALDESI imaging

Establishing an accurate *z*-resolution is pivotal for maintaining a consistent focus during 3D imaging with

IR-MALDESI. This is particularly vital given the Gaussian profile of the laser, which tends to lose focus over time, especially as material is progressively ablated from the samples. To quantify the *z*-resolution, laser ablation was carried out on healthy skin biopsies for 5, 10, and 20 layers. The subsequent ablated craters were analyzed with the VK-X1100 Keyence Confocal microscope. Graphing the ablation depth against the respective layer numbers, the derived slope gave an average depth per layer, effectively denoting the *z*-resolution. Utilizing a laser energy between 0.4 and 0.5 mJ, the *z*-resolution was found to be approximately 9  $\mu\text{m}$  (Supplemental Fig. 1). This crucial information now serves as a guide for the *z*-stage movement in 3D imaging, preserving laser focus integrity throughout the process.

Having established the *z*-resolution, a detailed 40-layer imaging experiment was performed on biopsies from three distinct healthy mice to validate the repeatability of the IR-MALDESI imaging methodology. Cholesterol ion, identified as  $[\text{M} + \text{H} - \text{H}_2\text{O}]^+$  with *m/z* 369.3516, served as a reference molecule for this validation. Heatmaps, as depicted in Fig. 2a, illustrate the cholesterol abundance and its consistent distribution across different skin layers. Despite originating from diverse samples, the cholesterol distribution patterns exhibit remarkable consistency, showcasing a descending abundance gradient from the epidermis through to the dermis and finally the hypodermis. However, owing to the inherent unevenness of murine skin, minor discrepancies in cholesterol levels were noted within the initial three layers across the samples, as visualized in Fig. 2b. These minor variations notwithstanding, the overarching abundance trends were consistent, underscoring the repeatability of the IR-MALDESI imaging system for biological applications. It is worth noting that in the biopsy from the first mouse, periodic abundance disruptions were observed at every 10-layer interval, potentially stemming from variations in laser fluence due to intermittent stage adjustments.

### Lipidomic profile during wound healing

Initial analysis centered on the comparison of spectra between wounded controls and their healthy counterparts during inflammation. Distinct discrepancies were noted in the abundance profiles of ceramide (Cer), phosphatidylcholine (PC), and phosphatidylethanolamine (PE) within the epidermal region, as depicted in Fig. 3a. Ceramides, which constitute approximately half of the stratum corneum's mass when combined with cholesterol and free fatty acids, are pivotal to the structural and functional integrity of this outermost epidermal layer. A compromised stratum corneum, due to ceramide dysregulation, can manifest as disrupted skin barrier functions, imbalanced homeostasis, and escalated trans-epithelial water loss. Beyond their structural role, ceramides also modulate inflammatory responses, being integral

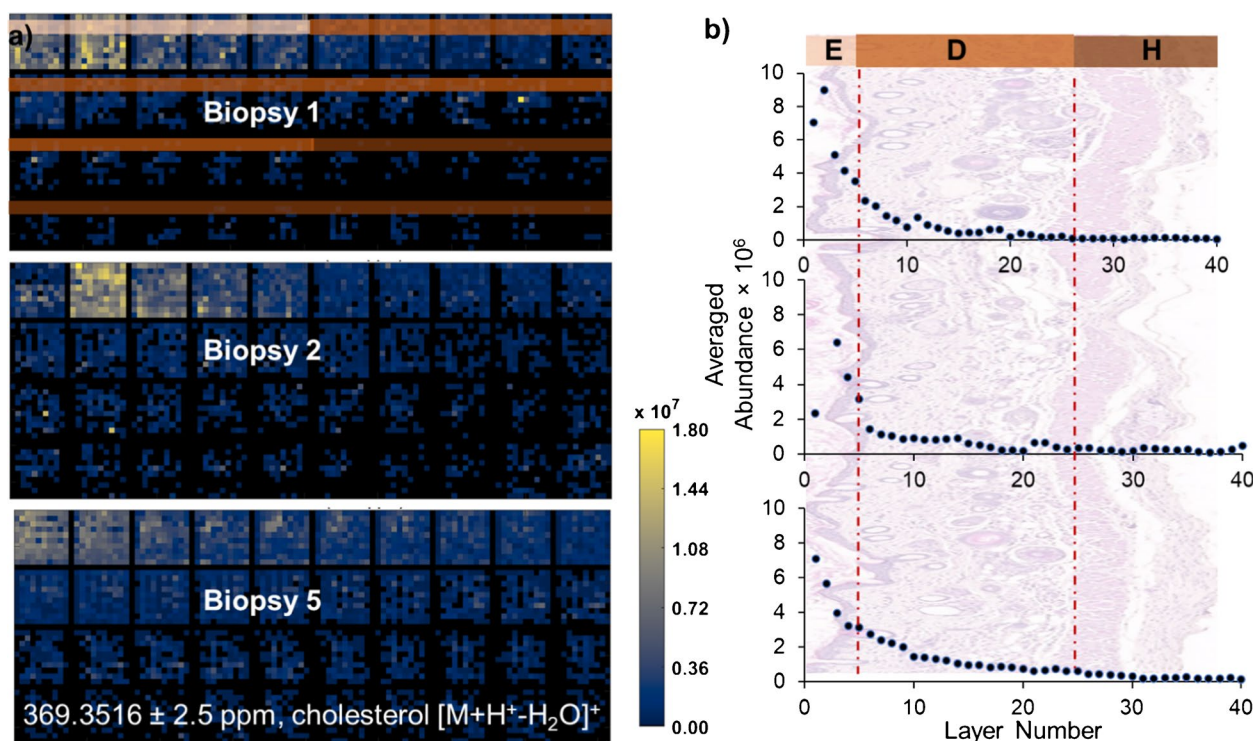


**Fig. 2** MSI analysis of cholesterol with IR-MALDESI, shown as  $[M + H^+ - H_2O]^+$  at  $m/z$  369.3516. **a** Heatmaps display the 3D distributions of cholesterol across three biopsy samples, demonstrating reproducibility despite inherent biological variability. **b** Graphical representation of cholesterol abundance against layer number.

The labels E, D, and H correspond to the epidermis, dermis, and hypodermis layers, respectively, and correlate to the appropriate skin anatomy in the background of the graph

membrane components that react to exogenous stimuli [40]. The heightened ceramide abundance in wounded skin may suggest an amplification of these processes. The heatmap for a representative ceramide, Cer (42:2), showcases its pronounced presence in wounded sites relative to healthy controls (Supplemental Fig. 2a). This particular ceramide species, previously identified in macrophages of mice, is reportedly accentuated during macrophage activation [41]. While ceramide and its derivatives have been integral in various cellular activities, ceramide-1-phosphate (C1P) stands out for its roles in fibroblast mobility, mast cell activation, and inflammation mediation [42]. In our study, a subtle increase in C1P was observed in the wound environment compared to the normal tissue (Supplemental Fig. 2b). These observations align with prior research suggesting that the dynamics of C1P during wound healing might differentiate wound tissue from normal tissue. However, the differences in our dataset were not as pronounced as might be expected based on previous findings, underscoring the need for further investigation.

In the dermal layer, a pronounced abundance of sebaceous glands is observable, consistent with the elevated levels of diglycerides (DG) and triglycerides (TG) depicted in Fig. 3b. DGs, as key intermediates in lipid metabolism, are involved in the synthesis of TGs and may also influence

cellular signaling pathways that regulate inflammation and tissue repair during wound healing. However, the specific mechanisms by which DGs contribute to this process remain unclear and warrant further investigation. TGs are known for their roles in proliferation and adaptive immunity, but still remains underexplored concerning their specific contribution during wound healing. Notably, TGs can be converted into acetyl-CoA, providing ATP to meet the energy demands of the wound repair process. Past efforts have even documented the utility of lipid concoctions rich in TG in facilitating wound repair [43].

To gain deeper insights into the lipidomic alterations in wounded samples, unique ions from representative layers were delineated and subjected to pathway analysis, revealing overarching shifts across the skin's various layers. Lipid candidates were identified using LipidsMaps based on molecular formula matches (Supplemental Table 1) and were evaluated through functional enrichment analysis, with the dominant pathways delineated in Table 1. Significant pathway enrichment was predominantly observed in the epidermis, including glycerophospholipid (GPL) metabolism, choline metabolism, ether lipid metabolism, fat digestion and absorption, and sphingolipid (SP) signaling. Given the established roles of GPLs in both intra- and intercellular communications, their prominence in wounded samples



tive to the healthy biopsy. In contrast, the dermis of layer 10 reveals increased abundance of diglycerides (DG) and triglycerides (TG) in the wounded skin, but diminished levels of PE and its species. These variances in lipid composition underscore the potential modifications in lipid metabolism and signaling intrinsic to the wound healing process

While lipidomics offers a detailed view of lipid distribution and composition across skin layers, proteomics provides insight into the intricate proteomics molecular responses of the skin during different phases of wound healing. Proteomics has been an essential tool in wound healing research, shedding light on complex molecular pathways and mechanisms

Layer	Unique lons	Pathway name	p-value	Benjamini correction
1	364	<b>Glycerophospholipid metabolism</b>	<b>4.42175E-07</b>	<b>1.54761E-05</b>
		<b>Choline metabolism</b>	<b>0.000860367</b>	<b>0.015056428</b>
		<b>Ether lipid metabolism</b>	<b>0.00469932</b>	<b>0.041119053</b>
		<b>Fat digestion and absorption</b>	<b>0.004382789</b>	<b>0.041119053</b>
		<b>Sphingolipid signaling pathway</b>	<b>0.006370232</b>	<b>0.044591625</b>
		Necroptosis	0.011974096	0.059870479
		Ferroptosis	0.011749516	0.059870479
		Phospholipase D signaling pathway	0.038406952	0.168030414
		Retrograde endocannabinoid signaling	0.049748339	0.193465764
		Sphingolipid metabolism	0.069255849	0.242395471
		Glycerolipid metabolism	0.1526749	0.242891887
		..... (other 24)	....	...
10	220	Ether lipid metabolism	0.002495	0.002495
20	137	Not listed as lipids in KEGG BRITE or there are not pathways associated with lipids		
30	411	Ether lipid metabolism	0.0024945	0.0024945
40	389	Ether lipid metabolism	0.002495	0.002495

**Table 1** Pathways enriched in distinct skin layers identified from lipidomic analysis. This table summarizes the key pathways identified from lipidomic analysis of wounded samples. Observed pathway enrichment was predominantly found in the epidermis, suggesting its

role as a primary metabolic hub during the wound healing process. These findings represent preliminary insights and require further validation to confirm their biological significance

that guide the healing process [44, 45]. Through evaluating the roles of inflammatory mediators, growth factors, extracellular matrix proteins, and immune cell activity, previous proteomic studies have advanced our understanding of wound progression and highlighted potential therapeutic targets [45].

In this study, our proteomic analysis aimed to elucidate the temporal variations in protein expression throughout wound healing process under standard treatment with Woun'Dres [28]. A secondary objective of our study was to explore the potential molecular mechanisms underlying those changes. By identifying differential protein expression, we sought to characterize how the wound healing process evolves across its distinct stages (Supplemental Table 2).

Principal component analysis (PCA) revealed clear proteomic distinctions among the different stages of wound healing (Fig. 4a). Each stage, defined by specific molecular and cellular interactions, formed distinct separate clusters in the PCA plot, echoing findings from previous studies that analyzed wound healing stages in human samples [46]. Notably, the inflammation phase exhibited a unique proteomic signature, characterized by differential expression of pro-inflammatory mediators, immune cell markers, and enzymes involved in oxidative stress. This phase, marked by a surge in metabolic activity, is a critical juncture in wound healing. It sets the stage for the following processes, coordinating

the interplay of proteins and molecular pathways to initiate immune response, tissue repair, and regeneration [46, 47].

Although clear clustering was observed with PCA, Venn diagram analysis (Fig. 4b) highlights that out of the 4828 proteins identified in this study, 4259 (88.2%) are expressed across all stages of wound healing and healthy skin. This finding underscores that it is the relative abundance and dynamic changes within the protein network, rather than the mere presence of individual proteins, drive the temporal phase of wound healing [46].

Based on Fig. 4b and Supplemental Table 3, we have identified 27 uniquely expressed proteins during the inflammation stage. Among these, several members of the Small Proline-Rich Protein (SPRR) family—Sprr2 h, Sprr2k, Sprr2b, Sprr2 g, and Sprr2 d—were identified. These proteins are known to play crucial roles in maintaining epidermal homeostasis and providing protection against bacterial invasion, underscoring their relevance in skin barrier function [48].

Additionally, three members of the Rho GTPase Activating Protein family—Arhgap32, Arhgap33, and Arhgap31—were uniquely expressed during the inflammatory phase. Rho GTPase Activating Proteins are known to regulate Rho GTPases, which are involved in cytoskeletal remodeling during cell wound repair [49]. Additionally, Rho GTPases have



**Table 2** Upregulated lipid-related proteins during the inflammation stage in wound control. The majority are lipoproteins, with those presented in italics representing enzymes integral to the arachidonic acid pathway

Protein name	Function
Aldehyde dehydrogenase 9, subfamily A1	Enables oxidoreductase activity, acting on the aldehyde or oxo group of donors, NAD or NADP as acceptor
<i>Arachidonate 5-lipoxygenase activating protein</i>	<i>Synthesis of leukotrienes</i>
1-acylglycerol- 3-phosphate O-acyltransferase 4	Enables 1-acylglycerol- 3-phosphate O-acyltransferase activity
Annexin A1	Phospholipase A2 inhibitor activity
Apolipoprotein A-IV	Anti-inflammatory
Apolipoprotein B	Lipids Transporter
Apolipoprotein B receptor	Enables very-low-density lipoprotein particle receptor activity
Apolipoprotein C-I	Activation of esterified lecithin cholesterol
Apolipoprotein C-IV	Lipids Transporter
Apolipoprotein E	Lipids Transporter
Apolipoprotein H	Regulatory role in coagulation, lipids binding
$\alpha$ - 2-glycoprotein 1, zinc	Stimulates lipolysis
Biotinidase	Recycle of vitamin biotin
Clusterin	Lipid transport, modulate the activity of leptin
Coenzyme Q2 homolog, prenyltransferase (yeast)	Glycerol metabolic process and ubiquinone biosynthetic process
Cellular retinoic acid binding protein I	Retinoic acid-mediated differentiation and proliferation processes
DnaJ (Hsp40) homolog, subfamily A, member 1	Stimulates ATP hydrolysis
GC vitamin D binding protein	Actin binding activity and calcidiol binding activity
Group specific component	Transports vitamin D and its metabolites
Glycosylphosphatidylinositol specific phospholipase D1	Releasing the attached protein from the plasma membrane
Glutathione peroxidase 3	Response to lipid hydroperoxide
Lipopolysaccharide binding protein	Elicit immune responses
<i>Leukotriene A4 hydrolase</i>	<i>Arachidonic acid metabolism</i>
Macrophage scavenger receptor 1	Enables amyloid-beta binding activity
Neutrophil cytosolic factor 1	Active in phagocytes
Phospholipase A2, group VII (platelet-activating factor acetylhydrolase, plasma)	Phospholipids binding activity
Phospholipid transfer protein	Enables lipid transfer activity
Protein kinase C, $\delta$	Regulate immunity (regulates the production of interleukin- 12 (IL- 12) p40/70 in both macrophages and dendritic cells)
Retinol binding partner 4	Transferring retinol
Paraoxonase 1	Enables arylesterase activity
<i>Prostaglandin I2 (prostacyclin) synthase</i>	<i>Synthesis of cholesterol, steroids and other lipids</i>
Serine (or cysteine) peptidase inhibitor, clade A, member 6	Major transport protein for glucocorticoids and progestins
STT3, subunit of the oligosaccharyltransferase complex, homolog A ( <i>S. cerevisiae</i> )	Enable dolichyl-diphosphooligosaccharide-protein glycotransferase activity
Solute carrier family	Membrane transport

been implicated in the migration, activation, differentiation, and apoptosis of immune cells in other inflammatory diseases contexts, such as inflammatory bowel disease [50].

Interestingly, two proteins that are uniquely expressed in inflammation are associated with lipid metabolism: Pla2 g4e (Phospholipase A2, Group IVE) and Apolipoprotein M (ApoM). ApoM is an apolipoprotein that regulates sphingosine- 1-phosphate (S1P), which plays a critical role in cell signaling related to inflammation and wound healing. Pla2 g4e, a phospholipase, is responsible for the release of

arachidonic acid, a precursor for inflammatory mediators [51]. These findings suggest potential roles for lipid metabolism in coordinating inflammatory responses during wound healing, though further studies are needed to fully elucidate these mechanisms.

We employed volcano plots to compare treated samples with healthy controls using a significance threshold of p-value < 0.05 and a fold change of 2 (Fig. 5a and Supplemental Table 4). The inflammation phase exhibited the most notable changes during healing, with 1,356 downregulated

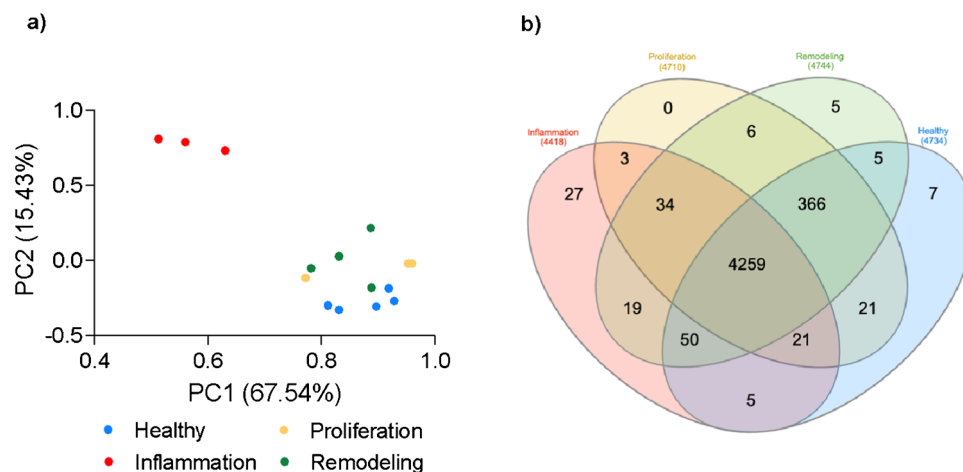


**Fig. 4** Distinct proteomic landscapes across wound healing stages visualized through PCA and Venn's diagram. **a** This PCA plot captures the unique proteomic signatures characteristic of each wound healing stage. Samples are clustered based on their molecular interactions and expression profiles. This figure underscores the inflamma-

tion phase as a pivotal moment in wound healing, driving metabolic surges and orchestrating subsequent stages of tissue repair and regeneration. **b** Venn's diagram comparing each stage of wound healing process with healthy unwounded skin

and 675 upregulated proteins. In comparison, the proliferation stage showed 128 downregulated and 186 upregulated proteins, while the remodeling stage exhibited 402 downregulated and 422 upregulated proteins.

Gene ontology analysis using Ranked-Based Testing (Fig. 5b and Supplemental Table 5) highlighted

stage-specific enrichment patterns. During the inflammation stage, 248 GO-terms were significantly enriched. These terms were primarily associated with immune response (GO:0002253, GO:0006954), bias towards a humoral response (GO:0006959, GO:0002455), as well as pathways associated with the coagulation cascade (GO:0007596) and

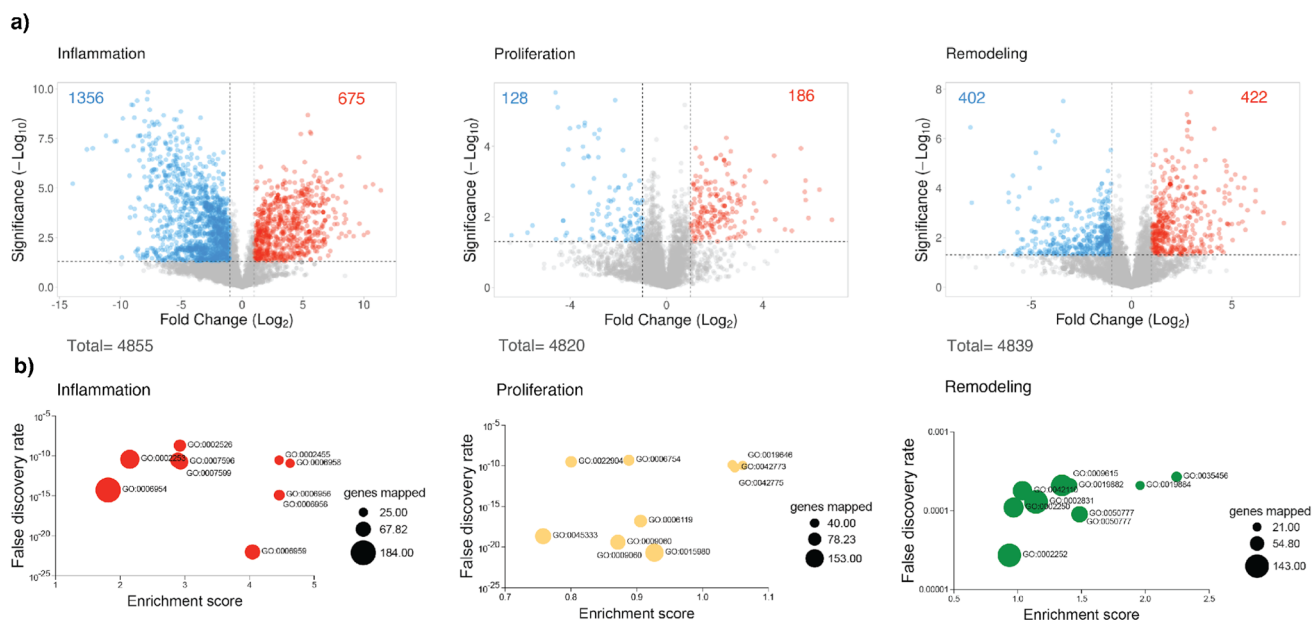


**Fig. 5** Differential protein expression across wound healing stages. **a** Volcano plots showing differential protein expression across the phases of wound healing. Wounded samples compared to normal tissue during the inflammation, proliferation, and regeneration phases of wound healing. Each dot represents a protein, with its position indicating the extent of change (x-axis) and the statistical significance of

that change (y-axis). The plots provide insight into the unique molecular responses and potential therapeutic effects of treatments in the context of wound healing progression. **b** Bubble plots displaying the biological functions (Gene ontology) with the highest upregulation in each stage of wound healing

hemostasis (GO:0007599). These results align with the cellular biology process described in this stage, where hemostasis creates a blood clot as the primary barrier following injury, and an immediate immune response triggers an acute humoral and inflammatory activity [39].

The proliferation stage exhibited 106 significantly enriched GO-terms, with the most upregulated terms associated with cellular respiration (GO:0045333) and ATP biosynthesis process (GO:0006754). These results are consistent with active metabolic activity during this stage, driven by the migration and recruitment of fibroblasts, endothelial cells, and keratinocytes to the wound site [52].

Finally, the remodeling phase displayed 148 significantly enriched GO-terms, with the most upregulated terms linked to adaptive immune response (GO:0002250) and T-cell activation (GO:0042110). This stage reflects a shift in cytokine profiles and the presence of adaptive immune cells, which help promote tissue regeneration and regulate the behavior of cells such as fibroblasts. These processes contribute to the deposition and the remodeling of extracellular matrix components during wound repair [53].

## Integration of proteomics and lipidomics

The integration of lipidomics and proteomics provides a lens through which we can offer a valuable framework for exploring the molecular dynamics of wound healing, particularly the interplay between lipids and proteins during the healing process. Proteomic analysis highlighted the significance of proteins involved in inflammation, prompting a focused examination of the upregulated protein set during this phase. Harnessing the LipidsMaps Proteome Database (LMPD) enabled us to identify lipid-related proteins among this upregulated set, revealing key actors in lipid metabolism.

Beyond their well-recognized roles as cellular membrane constituents, lipids play pivotal roles in signaling, energy storage, and regulation of cellular processes [54]. Our integrated lipid-related proteins analysis highlights the multifaceted functions of these lipid functions. Specifically, we identified proteins associated with the biosynthesis of phosphatidylcholine (PC) and sphingolipids (SP), both of which are critical components of cellular membranes. In addition to biosynthesis, lipid transport proteins, such as fatty acid-binding proteins (FABPs) and lipid transfer proteins, underscore the intricate mechanisms facilitating efficient lipid transport within cellular environments.

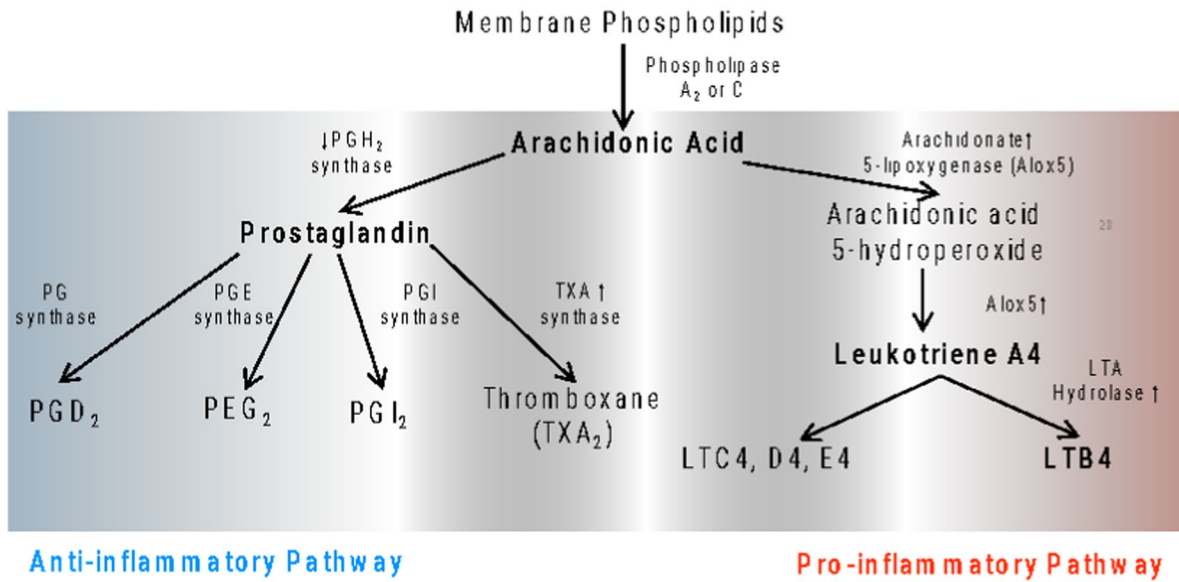
Moreover, our dataset reveals the significance of lipid-mediated signaling, particularly through the proteins involved in the phosphoinositide 3-kinase (PI3 K) pathway. The pronounced presence of these proteins during the inflammation aligns with the activities of neutrophils and

macrophages, key immune cells that play central roles in the wound healing process. While traditionally associated with host defense and infection, these immune cells are also deeply interconnected with lipid-mediated signaling processes, further emphasizing their diverse functional roles during inflammation and tissue repair.

In this analysis, a notable discovery was a group of proteins marked italicized in Table 2, which all belong to the eicosanoid pathway. As depicted in Fig. 6a, this pathway is centered around the transformation of arachidonic acid, a polyunsaturated fatty acid liberated from cell membranes via the activity of phospholipase A2 or C. This pathway has been previously implicated in wound healing process by numerous studies [55, 56]. Arachidonic acid serves as a precursor for various lipid mediators. Collaborating with PGH2 synthase, it can be converted into substances such as prostaglandins, thromboxanes, prostacyclins, and various other prostanoids, which majorly undertake anti-inflammatory functions [55]. On another route, the enzyme arachidonate 5-lipoxygenase directs arachidonic acid to form an intermediate, arachidonic acid 5-hydroperoxide (5-HETE), which subsequently turns to leukotriene A4 and B4 (LTB4) [56]. These pro-inflammatory lipid mediators contribute to the initiation and propagation of inflammation by activating platelet aggregation. The elevated abundance of enzymes involved in both anti-inflammatory and pro-inflammatory pathways emphasizes the complex interplay and signaling network within the wound healing process.

The lipid profiles shown in Fig. 6b, along with additional data, illustrate significant changes occurring in the samples. Notably, arachidonic acids exhibit heightened levels across all wounded specimens, indicating a shift in lipid metabolism associated with the wound healing process. The wounded samples also show increased levels of inflammation-promoting leukotriene A4, suggesting a more pronounced inflammatory response. This observation is consistent with the expected physiological reaction to wounding. The differential expression observed in the heatmaps of lipids from healthy and wounded skin can be explained by the differences in enzyme expression presented in Fig. 6c. Specifically, the increased expression of Alox5 and LTA4 h enzymes correlates with the pro-inflammatory environment in wounded samples, as evidenced by the higher levels of leukotriene A4. Alox5 (5-lipoxygenase) plays a crucial role in the biosynthesis of leukotrienes from arachidonic acid [57], while LTA4 h (Leukotriene A4 hydrolase) catalyzes the conversion of leukotriene A4 to leukotriene B4, a potent inflammatory mediator [58]. The upregulation of these enzymes explains the elevated leukotriene A4 levels observed in the wounded samples. These findings underscore the complex and tightly regulated inflammatory response during wound healing, highlighting how molecular-level changes in lipid metabolism

a)

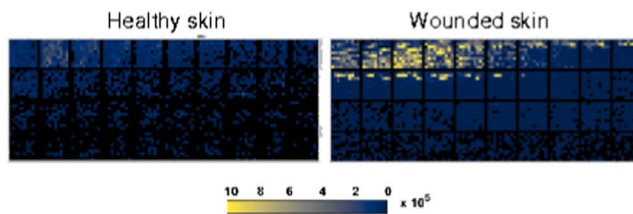


Anti-inflammatory Pathway

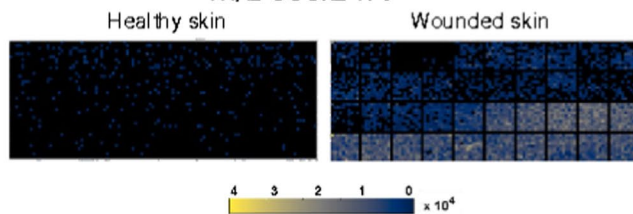
Pro-inflammatory Pathway

b)

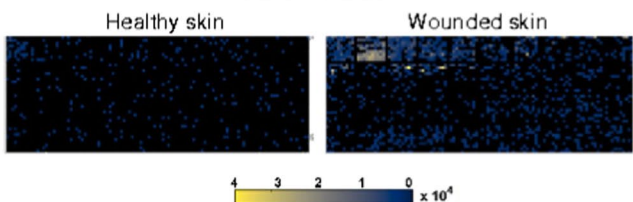
**Arachidonic Acid**  
m/z 305.2475



**Prostaglandin**  
m/z 355.2479



**Leukotriene A4**  
m/z 319.2268



c)

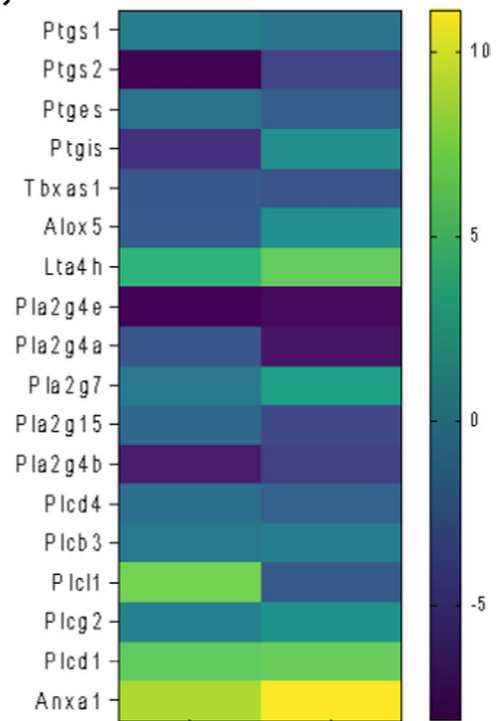


**Fig. 6** Significance of the arachidonic acid pathway in wound healing. **a** schematic representation of the arachidonic acid pathway, highlighting its bifurcation into two distinct sub-pathways involved in inflammation regulation. **b** 3D heatmaps present the spatial distribution of differentially regulated lipids within the arachidonic pathway.

These heatmaps provide a comparative analysis, emphasizing the differences in microenvironments observed in healthy against wounded skin. **c** Heatmap of the enzymes associated with arachidonic acid pathway



and enzyme activity contribute to the broader physiological response to wound healing.

The evolution of multi-omics approaches is at the forefront of reshaping how we understand complex physiological processes like wound healing. The ability to overlay different data landscapes offers a holistic perspective, enabling a detailed exploration of the intricate relationships between cellular events and molecular signaling pathways. Our research, by focusing on the integration of spatial resolved lipidomics and temporal proteomics, presents a methodology with potential applicability to a myriad of biological phenomena, not limited to wound healing alone.

A key insight from our study underscores the pivotal role of inflammation in wound healing, as illuminated by our proteomics analysis. The findings emphasize the necessity of regulating inflammation for optimal recovery. Additionally, the spatially resolved lipidomics study sheds light on the epidermis as an intensely active participant in the wound healing process. Utilizing the entire wound sample for lipidomics could have overlooked these specific epidermal contributions, highlighting the indispensability of 3D analytical methodologies in discerning spatial heterogeneities.

It is important to note that the arachidonic acid pathway highlighted has been previously implicated in the inflammatory stage of wound healing by numerous studies [55, 56]. Our findings do not represent a new discovery of this pathway's involvement, but rather provide additional validation through a multi-omics approach. By combining spatially resolved lipidomics with temporally resolved proteomics, we offer a more comprehensive view of how this established pathway functions within the broader context of wound healing. This integrated approach allows us to observe the interplay between lipid mediators and their associated proteins, providing a deeper understanding of the molecular dynamics at play.

However, it is pertinent to note that while our emphasis on lipid-related proteomics has revealed valuable insights, it only scratches the surface of the potential that integrated multi-omics holds. One potential limitation of our study is the chosen approach itself. Vertical analyte delocalization remains a potential concern in 3D MSI experiments. Future studies should incorporate reverse-orientation imaging to validate the spatial distribution of analytes from the hypodermis to the epidermis. Although not performed here, such approaches would provide a more robust assessment of analyte localization and mitigate potential artifacts. Also, by prioritizing lipid-related proteomics, we may have inadvertently sidelined other important proteins or pathways that could be equally instrumental in the wound healing process. Furthermore,

other multi-omics layers—like transcriptomics, genomics, or metabolomics—could also provide invaluable context and depth, creating a more comprehensive narrative. This work, while methodologically focused, would benefit immensely from being underpinned by more extensive biological data. Another limitation is the sample size. Greater biological replicates would lend more statistical power and robustness to our findings. While our results are promising, broadening the sample pool in future research will better cement the relationships and trends we have identified. Our approach demonstrates the potential of integrated multi-omics not just for pathway discovery, but for providing deeper insights into complex biological processes. By combining spatial lipidomics with temporal proteomics, we offer a methodology that could be applied to various biological phenomena during wound healing.

## Conclusions

The study of wound healing was conducted using a comprehensive multi-dimensional approach, encompassing spatial, temporal, and multi-omics analyses. The spatially resolved lipidomic profiles provided insights into the distinct molecular compositions of the epidermis, dermis, and hypodermis during the wound healing process. Enrichment analysis further emphasized the significant biological activity observed in the epidermis, highlighting its crucial role in wound healing. Temporally resolved proteomics revealed dynamic changes across all three treatment groups, with a clear indication that the inflammation stage represents the most active phase in the wound healing process. The integration of multi-omics data was exemplified through a robust examination of arachidonic acid and its metabolic pathway, showcasing the potential of this approach for comprehensive molecular investigations. Moving forward, future efforts will be directed towards enhancing the system and advancing data interpretation techniques, enabling a deeper understanding of wound healing mechanisms.

**Supplementary Information** The online version contains supplementary material available at <https://doi.org/10.1007/s00216-025-05865-5>.

**Acknowledgements** All mass spectrometry measurements were conducted in the Molecular Education, Technology and Research Innovation Center (METRIC) at North Carolina State University.

**Author contribution** Conceptualization, D.M. and T.S.; methodology, H.B. and D.M.; investigation, H.B. A.S.A. and Y.L.; visualization, H.B.; writing — original draft, H.B. and A.S.A.; writing — review and editing, D.M. and T.S.; funding acquisition, D.M. and T.S.; resources, D.M. and T.S.

**Funding** The authors received financial support from the National Institutes of Health (R01GM087964).

## Declarations

**Ethical approval** All procedures were approved by the Duke University Institutional Animal Care and Use Committee and followed the NIH Guide for the Care and Use of Laboratory Animals.

**Conflict of interest** The authors declare the following competing financial interests: MSiReader was used in-part for the data analysis presented in this manuscript, and D.M. is a part owner of MSI Software Solutions, LLC. The authors have no other competing interests to disclose.

D.M. is currently member of ABC's International Advisory Board but was not involved in the peer review of this paper.

**Open Access** This article is licensed under a Creative Commons Attribution 4.0 International License, which permits use, sharing, adaptation, distribution and reproduction in any medium or format, as long as you give appropriate credit to the original author(s) and the source, provide a link to the Creative Commons licence, and indicate if changes were made. The images or other third party material in this article are included in the article's Creative Commons licence, unless indicated otherwise in a credit line to the material. If material is not included in the article's Creative Commons licence and your intended use is not permitted by statutory regulation or exceeds the permitted use, you will need to obtain permission directly from the copyright holder. To view a copy of this licence, visit <http://creativecommons.org/licenses/by/4.0/>.

## References

- Beldon P (2010) Basic science of wound healing. *Surgery* 28:409–412. <https://doi.org/10.1016/j.mpsur.2010.05.007>.
- Lindley LE, Stojadinovic O, Pastar I, Tomic-Canic M. Biology and biomarkers for wound healing. *Plast Reconstr Surg*. 2016;138:18S–28S. <https://doi.org/10.1097/PRS.00000000000002682>.
- Sen CK, Gordillo GM, Roy S, Kirsner R, Lambert L, Hunt TK, Gottrup F, Gurtner GC, Longaker MT. Human Skin Wounds: A Major Snoballing Threat to Public Health and Economy. *Wound Repair Regen*. 2010;17:763–71. <https://doi.org/10.1111/j.1524-475X.2009.00543.x.Human>.
- Kalkhof S, Förster Y, Schmidt J, Schulz MC, Baumann S, Weißflog A, Gao W, Hempel U, Eckelt U, Rammelt S, Von Bergen M. Proteomics and metabolomics for in situ monitoring of wound healing. *Biomed Res Int* 2014. <https://doi.org/10.1155/2014/934848>.
- Mascharak S, Talbott HE, Januszyk M, Griffin M, Chen K, Davitt MF, Demeter J, Henn D, Bonham CA, Foster DS, Mooney N, Cheng R, Jackson PK, Wan DC, Gurtner GC, Longaker MT. Multi-omic analysis reveals divergent molecular events in scarring and regenerative wound healing. *Cell Stem Cell*. 2022;29:315–327.e6. <https://doi.org/10.1016/j.stem.2021.12.011>.
- Jia Z, Liu L, Zhang S, Zhao X, Luo L, Tang Y, Shen B, Chen M. Proteomics changes after negative pressure wound therapy in diabetic foot ulcers. *Mol Med Rep*. 2021;24. <https://doi.org/10.3892/mmr.2021.12474>.
- Buchberger AR, DeLaney K, Johnson J, Li L. Mass Spectrometry Imaging: A Review of Emerging Advancements and Future Insights. *Anal Chem*. 2018;90:240–65. <https://doi.org/10.1021/acs.analchem.7b04733>.
- Kertesz V, Cahill JF. Spatially resolved absolute quantitation in thin tissue by mass spectrometry. *Anal Bioanal Chem*. 2021;413:2619–36.
- Seeley EH, Caprioli RM. 3D imaging by mass spectrometry: A new frontier. *Anal Chem*. 2012;84:2105–10. <https://doi.org/10.1021/ac2032707>.
- Dreisewerd K. Recent methodological advances in MALDI mass spectrometry. *Anal Bioanal Chem*. 2014;406:2261–78. <https://doi.org/10.1007/s00216-014-7646-6>.
- Fletcher JS, Lockyer NP, Vickerman JC. Developments in molecular SIMS depth profiling and 3D imaging of biological systems using polyatomic primary ions. *Mass Spectrom Rev*. 2011;30:142–74. <https://doi.org/10.1002/mas.20275>.
- Fletcher JS, Vickerman JC. A new SIMS paradigm for 2D and 3D molecular imaging of bio-systems. *Anal Bioanal Chem*. 2010;396:85–104.
- Bai H, Khodjaniyazova S, Garrard KP, Muddiman DC. Three-Dimensional Imaging with Infrared Matrix-Assisted Laser Desorption Electrospray Ionization Mass Spectrometry. *J Am Soc Mass Spectrom*. 2020;31:292–7. <https://doi.org/10.1021/jasms.9b00066>.
- Bai H, Linder KE, Muddiman DC. Three-dimensional (3D) imaging of lipids in skin tissues with infrared matrix-assisted laser desorption electrospray ionization (MALDESI) mass spectrometry. *Anal Bioanal Chem*. 2021;413:2793–801. <https://doi.org/10.1007/s00216-020-03105-6>.
- Pils V, Terlecki-Zaniewicz L, Schosserer M, Grillari J, Lämmermann I. The role of lipid-based signalling in wound healing and senescence. *Mech Ageing Dev*. 2021;198. <https://doi.org/10.1016/j.mad.2021.111527>.
- Yasukawa K, Okuno T, Yokomizo T. Eicosanoids in skin wound healing. *Int J Mol Sci*. 2020;21:1–19.
- Dhall S, Wijesinghe DS, Karim ZA, Castro A, Vemana HP, Khasawneh FT, Chalfant CE, Martins-Green M. Arachidonic acid-derived signaling lipids and functions in impaired healing. *Wound Repair Regen*. 2015;23:644–56. <https://doi.org/10.1111/wrr.12337>.
- Menon R, Krzyszczyk P, Berthiaume F. Pro-Resolution Potency of Resolvins D1, D2 and E1 on Neutrophil Migration and in Dermal Wound Healing. *Nano Life*. 2017;07:1750002. <https://doi.org/10.1142/s1793984417500027>.
- Fernandez ML, Broadbent JA, Shooter GK, Malda J, Upton Z. Development of an enhanced proteomic method to detect prognostic and diagnostic markers of healing in chronic wound fluid. *Br J Dermatol*. 2008;158:281–90. <https://doi.org/10.1111/j.1365-2133.2007.08362.x>.
- Amit Gefen. Bioengineering research of chronic wounds : a multidisciplinary study approach. Berlin: Springer; 2009.
- Rayment EA, Upton Z. Review: Finding the culprit: A review of the influences of proteases on the chronic wound environment. *Int J Lower Extrem Wounds*. 2009;8:19–27.
- Clarke HA, Ma X, Shedlock CJ, Medina T, Hawkinson TR, Wu L, Ribas RA, Keohane S, Ravi S, Bizon J, Burke S, Abisambra JF, Merritt M, Prentice B, Vander Kooi CW, Gentry MS, Chen L, Sun RC. Spatial Metabolome Lipidome and Glycome from a Single brain Section. *bioRxiv*. 2023;13:4327. <https://doi.org/10.1101/2023.07.22.550155>.
- Tian H, Rajbhandari P, Tarolli J, Decker AM, Neelakantan TV, Angerer T, Zandkarimi F, Remotti H, Frache G, Winograd N, Stockwell BR. Multimodal mass spectrometry imaging identifies cell-type-specific metabolic and lipidomic variation in the mammalian liver. *Dev Cell*. 2024;59:869–881.e6. <https://doi.org/10.1016/j.devcel.2024.01.025>.
- Zhang H, Lu KH, Ebbini M, Huang P, Lu H, Li L. Mass spectrometry imaging for spatially resolved multi-omics molecular mapping. *npj Imaging*. 2024;2. <https://doi.org/10.1038/s44303-024-00025-3>.
- Cassat JE, Moore JL, Wilson KJ, Stark Z, Prentice BM, Van de Plas R, Perry WJ, Zhang Y, Virostko J, Colvin DC, Rose KL,

- Judd AM, Reyzer ML, Spraggins JM, Grunenwald CM, Gore JC, Caprioli RM, Skaar EP. Integrated molecular imaging reveals tissue heterogeneity driving host-pathogen interactions. *J Sci Transl Med*. 2018;10. <https://doi.org/10.5061/dryad.q9080>.
26. Jain S, Pei L, Spraggins JM, Angelo M, Carson JP, Gehlenborg N, Ginty F, Gonçalves JP, Hagood JS, Hickey JW, Kelleher NL, Laurent LC, Lin S, Lin Y, Liu H, Naba A, Nakayasu ES, Qian WJ, Radtke A, Robson P, Stockwell BR, Van de Plas R, Vlachos IS, Zhou M, Ahn KJ, Allen J, Anderson DM, Anderton CR, Curcio C, Angelin A, Arvanitis C, Atta L, Awosika-Olumo D, Bahmani A, Bai H, Balderrama K, Balzano L, Bandyopadhyay G, Bandyopadhyay S, Bar-Joseph Z, Barnhart K, Barwinska D, Becich M, Becker L, Becker W, Bedi K, Bendall S, Benninger K, Betancur D, Bettinger K, Billings S, Blood P, Bolin D, Border S, Bosse M, Bramer L, Brewer M, Brusko M, Bueckle A, Burke K, Burnum-Johnson K, Butcher E, Butterworth E, Cai L, Calandrelli R, Caldwell M, Campbell-Thompson M, Cao D, Cao-Berg I, Caprioli R, Caraccio C, Caron A, Carroll M, Chadwick C, Chen A, Chen D, Chen F, Chen H, Chen J, Chen L, Chen L, Chiacchia K, Cho S, Chou P, Choy L, Cisar C, Clair G, Clarke L, Clouthier KA, Colley ME, Conlon K, Conroy J, Contrepolis K, Corbett A, Corwin A, Cotter D, Courtois E, Cruz A, Csonka C, Czupil K, Daiya V, Dale K, Davanagere SA, Dayao M, de Caestecker MP, Decker A, Deems S, Degnan D, Desai T, Deshpande V, Deutsch G, Devlin M, Diep D, Dodd C, Donahue S, Dong W, dos Santos Peixoto R, Duffy M, Dufresne M, Duong TE, Dutra J, Eadon MT, El-Achkar TM, Ennifful A, Eraslan G, Eshelman D, Espin-Perez A, Esplin ED, Esselman A, Falo LD, Falo L, Fan J, Fan R, Farrow MA, Farzad N, Favaro P, Fermin J, Filiz F, Filus S, Fisch K, Fisher E, Fisher S, Flowers K, Flynn WF, Fogo AB, Fu D (Ann), Fulcher J, Fung A, Furst D, Gallant M, Gao F, Gao Y, Gaulton K, Gaut JP, Gee J, Ghag RR, Ghazanfar S, Ghose S, Gisch D, Gold I, Gondalia A, Gorman B, Greenleaf W, Greenwald N, Gregory B, Guo R, Gupta R, Hakimian H, Haltom J, Halushka M, Han KS, Hanson C, Harbury P, Hardi J, Harlan L, Harris RC, Hartman A, Heidari E, Helfer J, Helminiak D, Hemberg M, Henning N, Herr BW, Ho J, Holden-Wiltse J, Hong SH, Hong YK, Honick B, Hood G, Hu P, Hu Q, Huang M, Huyc K, Imtiaz T, Isberg OG, Itkin M, Jackson D, Jacobs M, Jain Y, Jewell D, Jiang L, Jiang ZG, Johnston S, Joshi P, Ju Y, Judd A, Kagel A, Kahn A, Kalavros N, Kalhor K, Karagkouni D, Karathanos T, Karunamurthy A, Katari S, Kates H, Kaushal M, Keener N, Keller M, Kenney M, Kern C, Kharchenko P, Kim J, Kingsford C, Kirwan J, Kiselev V, Kishi J, Kitata RB, Knoten A, Kollar C, Krishnamoorthy P, Kruse ARS, Da K, Kundaje A, Kutschera E, Kwon Y, Lake BB, Lancaster S, Langlieb J, Lardenoije R, Laronda M, Laskin J, Lau K, Lee H, Lee M, Lee M, Strelakova YL, Li D, Li J, Li J, Li X, Li Z, Liao YC, Liaw T, Lin P, Lin Y, Lindsay S, Liu C, Liu Y, Liu Y, Lott M, Lotz M, Lowery L, Lu P, Lu X, Lucarelli N, Lun X, Luo Z, Ma J, Macosko E, Mahajan M, Maier L, Makowski D, Malek M, Manthey D, Manz T, Margulies K, Marioni J, Martindale M, Mason C, Mathews C, Maye P, McCallum C, McDonough E, McDonough L, McDowell H, Meads M, Medina-Serpas M, Ferreira RM, Messinger J, Metis K, Migas LG, Miller B, Mimar S, Minor B, Misra R, Missarova A, Mistretta C, Moens R, Moerth E, Moffitt J, Molla G, Monroe M, Monte E, Morgan M, Muraro D, Murphy B (Robert), Murray E, Musen MA, Naglah A, Nasamran C, Neelakantan T, Nevins S, Nguyen H, Nguyen N, Nguyen T, Nguyen T, Nigra D, Nofal M, Nolan G, Nwanne G, O'Connor M, Okuda K, Olmer M, O'Neill K, Otoluka N, Pang M, Parast M, Pasa-Tolic L, Paten B, Patterson NH, Peng T, Phillips G, Pichavant M, Piehowski P, Pilner H, Pingry E, Pita-Juarez Y, Plevritis S, Ploumakis A, Pouch A, Pryhuber G, Puerto J, Qaurooni D, Qin L, Quardokus EM, Rajbandari P, Rakow-Penner R, Ramasamy R, Read D, Record EG, Reeves D, Ricarte A, Rodriguez-Soto A, Ropelewski A, Rosario J, Roselkis MA, Rowe D, Roy TK, Ruffalo M, Ruschman N, Sabo A, Sachdev N, Saka S, Salamon D, Sarder P, Sasaki H, Satija R, Saunders D, Sawka R, Schey K, Schlehlein H, Scholten D, Schultz S, Schwartz L, Schwenk M, Scibek R, Segre A, Ser-rata M, Shands W, Shen X, Shendure J, Shephard H, Shi L, Shi T, Shin DG, Shirey B, Sibilla M, Silber M, Silverstein J, Simmel D, Simmons A, Singhal D, Sivajothi S, Smits T, Soncin F, Song Q, Stanley V, Stuart T, Su H, Su P, Sun X, Surette C, Swahn H, Tan K, Teichmann S, Tejomay A, Tellides G, Thomas K, Thomas T, Thompson M, Tian H, Tideman L, Trapnell C, Tsai AG, Tsai CF, Tsai L, Tsui E, Tsui T, Tung J, Turner M, Uranic J, Vaishnav ED, Varra SR, Vaskivskyi V, Velickovic D, Velickovic M, Verheyden J, Waldrip J, Wallace D, Wan X, Wang A, Wang F, Wang M, Wang S, Wang X, Wasserfall C, Wayne L, Webber J, Weber GM, Wei B, Wei JJ, Weimer A, Welling J, Wen X, Wen Z, Williams MK, Winfree S, Winograd N, Woodard A, Wright D, Wu F, Wu PH, Wu Q, Wu X, Xing Y, Xu T, Yang M, Yang M, Yap J, Ye DH, Yin P, Yuan Z, Yun C (Jina), Zahraei A, Zemaitis K, Zhang B, Zhang C, Zhang C, Zhang C, Zhang K, Zhang S, Zhang T, Zhang Y, Zhao B, Zhao W, Zheng JW, Zhong S, Zhu B, Zhu C, Zhu D, Zhu Q, Zhu Y, Börner K, Snyder MP. Advances and prospects for the Human BioMolecular Atlas Program (HuBMAP). *Nat Cell Biol*. 2023;25:1089–1100. <https://doi.org/10.1038/s41556-023-01194-w>.
  27. Griffin DR, Archang MM, Kuan CH, Weaver WM, Weinstein JS, Feng AC, Ruccia A, Sideris E, Ragkousis V, Koh J, Plikus MV, Di Carlo D, Segura T, Scumpia PO. Activating an adaptive immune response from a hydrogel scaffold imparts regenerative wound healing. *Nat Mater*. 2021;20:560–9. <https://doi.org/10.1038/s41563-020-00844-w>.
  28. Liu Y, Suarez-Arnedo A, Caston ELP, Riley L, Schneider M, Segura T. Exploring the Role of Spatial Confinement in Immune Cell Recruitment and Regeneration of Skin Wounds. *Adv Mater*. 2023;35. <https://doi.org/10.1002/adma.202304049>.
  29. Knizner KT, Guymon JP, Garrard KP, Bouvrée G, Manni J, Hauschild J-P, Strupat K, Fort KL, Earley L, Wouters ER, Pu F, Radosevich AJ, Elsen NL, Williams JD, Pankow MR, Muddiman DC. Next-Generation Infrared Matrix-Assisted Laser Desorption Electrospray Ionization Source for Mass Spectrometry Imaging and High-Throughput Screening. *J Am Soc Mass Spectrom*. 2022. <https://doi.org/10.1021/jasms.2c00178>.
  30. Garrard KP, Ekelöf M, Khodjaniyazova S, Bagley MC, Muddiman DC. A Versatile Platform for Mass Spectrometry Imaging of Arbitrary Spatial Patterns. *J Am Soc Mass Spectrom*. 2020;31:2547–52. <https://doi.org/10.1021/jasms.0c00128>.
  31. Wiśniewski JR, Zougman A, Nagaraj N, Mann M. Universal sample preparation method for proteome analysis. *Nat Methods*. 2009;6:359–62. <https://doi.org/10.1038/nmeth.1322>.
  32. Bai H, Collins LB, André MR, Breitschwerdt EB, Williams TI. A bottom-up proteomics workflow for a system containing multiple organisms. *Rapid Commun Mass Spectrom*. 2023;38. <https://doi.org/10.1002/rcm.9431>.
  33. Schramm T, Hester A, Klinkert I, Both JP, Heeren RMA, Brunelle A, Laprévote O, Desbenoit N, Robbe MF, Stoeckli M, Spengler B, Römpp A. ImzML - A common data format for the flexible exchange and processing of mass spectrometry imaging data. *J Proteomics*. 2012;75:5106–10. <https://doi.org/10.1016/j.jprot.2012.07.026>.
  34. Bokhart MT, Nazari M, Garrard KP, Muddiman DC. MSiReader v1.0: Evolving Open-Source Mass Spectrometry Imaging Software for Targeted and Untargeted Analyses. *J Am Soc Mass Spectrom*. 2018;29:8–16. <https://doi.org/10.1007/s13361-017-1809-6>.
  35. Robichaud G, Garrard KP, Barry JA, Muddiman DC. MSiReader: An open-source interface to view and analyze high resolving power MS imaging files on matlab platform. *J Am Soc*

- Mass Spectrom. 2013;24:718–21. <https://doi.org/10.1007/s13361-013-0607-z>.
36. Fahy E, Sud M, Cotter D, Subramaniam S. LIPID MAPS online tools for lipid research. *Nucleic Acids Res.* 2007;35:606–12. <https://doi.org/10.1093/nar/gkm324>.
  37. Goedhart J, Luijsterburg MS. VolcanoR is a web app for creating, exploring, labeling and sharing volcano plots. *Sci Rep.* 2020;10. <https://doi.org/10.1038/s41598-020-76603-3>.
  38. Heberle H, Meirelles VG, da Silva FR, Telles GP, Minghim R. InteractiVenn: A web-based tool for the analysis of sets through Venn diagrams. *BMC Bioinformatics.* 2015;16. <https://doi.org/10.1186/s12859-015-0611-3>.
  39. Fitridge R, Thompson M, editors. Mechanisms of vascular disease: A reference book for vascular specialists [Internet]. Adelaide (AU): University of Adelaide Press. 2011. Available from: <https://www.ncbi.nlm.nih.gov/books/NBK534260/>
  40. Knox S, O'Boyle NM. Skin lipids in health and disease: A review. *Chem Phys Lipids.* 2021;236.
  41. Goto-Inoue N, Hayasaka T, Zaima N, Nakajima K, Holleran WM, Sano S, Uchida Y, Setou M. Imaging Mass Spectrometry Visualizes Ceramides and the Pathogenesis of Dorfman-Chanarin Syndrome Due to Ceramide Metabolic Abnormality in the Skin. *PLoS One.* 2012;7. <https://doi.org/10.1371/journal.pone.0049519>.
  42. Maus KD, Stephenson DJ, Ali AN, MacKnight HP, Huang HJ, Serrats J, Kim M, Diegelmann RF, Chalfant CE. Ceramide kinase regulates acute wound healing by suppressing 5-oxo-ETE biosynthesis and signaling via its receptor OXER1. *J Lipid Res.* 2022;63. <https://doi.org/10.1016/j.jlr.2022.100187>.
  43. Sonia Felício Magalhães MI, Vagnaldo Fecine FI, Nogueira de Macedo III R, Levi Silveira Monteiro III D, Carvalho Oliveira CI, Anne de Castro Brito G V, Elisabete Amaral de Moraes MV, Odorico de Moraes MV, Professor A. Effect of a combination of medium chain triglycerides, linoleic acid, soy lecithin and vitamins A and E on wound healing in rats 1 Efeito da combinação de triglicerídeos de cadeia média, ácido linoléico, lecitina de soja e vitaminas A e na cicatrização. 2008.
  44. Edsberg LE, Wyffels JT, Brogan MS, Fries KM. Proteomics of chronic pressure ulcers. *Wound Repair and Regeneration.* 2012;20:378–401. <https://doi.org/10.1111/j.1524-475X.2012.00791.x>.
  45. Broadbent J, Walsh T, Upton Z. Proteomics in chronic wound research: Potentials in healing and health. *Proteomics Clin Appl.* 2010;4:204–14.
  46. Gao X, Petricoin EF, Ward KR, Goldberg SR, Duane TM, Bonchev D, Arodz T, Diegelmann RF. Network proteomics of human dermal wound healing. *Physiol Meas.* 2018;39. <https://doi.org/10.1088/1361-6579/aace19>.
  47. Bioengineering research of chronic wounds: a multidisciplinary study approach. *Scholars Portal.* 2019.
  48. Zhang C, Hu Z, Lone AG, Artami M, Edwards M, Zouboulis CC, Stein M, Harris-Tryon TA. Small proline-rich proteins (SPRRs) are epidermally produced antimicrobial proteins that defend the cutaneous barrier by direct bacterial membrane disruption. *Elife.* 2022;11. <https://doi.org/10.7554/eLife.76729>.
  49. Verboon JM, Parkhurst SM. Rho family GTPases bring a familiar ring to cell wound repair. *Small GTPases.* 2015;6:1–7. <https://doi.org/10.4161/21541248.2014.992262>.
  50. Li X, Zhang M, Zhou G, Xie Z, Wang Y, Han J, Li L, Wu Q, Zhang S. Role of Rho GTPases in inflammatory bowel disease. *Cell Death Discov.* 2023;9.
  51. Gijón MA, Leslie CC. Regulation of arachidonic acid release and cytosolic Phospholipase A2 activation. *J Leukoc Biol.* 1999;65:330–6. <https://doi.org/10.1002/jlb.65.3.330>.
  52. Schiffmann LM, Werthenbach JP, Heintges-Kleinhofer F, Seeger JM, Fritsch M, Günther SD, Willenborg S, Brodesser S, Lucas C, Jüngst C, Albert MC, Schorn F, Witt A, Moraes CT, Bruns CJ, Pasparakis M, Krönke M, Eming SA, Coutelle O, Kashkar H. Mitochondrial respiration controls neoangiogenesis during wound healing and tumour growth. *Nat Commun.* 2020;11. <https://doi.org/10.1038/s41467-020-17472-2>.
  53. Cioce A, Cavani A, Cattani C, Scopelliti F. Role of the Skin Immune System in Wound Healing. *Cells.* 2024;13. <https://doi.org/10.3390/cells13070624>.
  54. Horn A, Jaiswal JK (2019) Structural and signaling role of lipids in plasma membrane repair. In: *Current Topics in Membranes*. Academic Press Inc., pp 67–98. <https://doi.org/10.1016/bs.ctm.2019.07.001>.
  55. Serhan CN, Yacoubian S, Yang R. Anti-inflammatory and proresolving lipid mediators. *Annu Rev Pathol.* 2008;3:279–312.
  56. Funk CD. (2001) Prostaglandins and leukotrienes: advances in eicosanoid biology. *Science.* 1979;294:1871–5.
  57. Assimes TL, Knowles JW, Priest JR, Basu A, Volcik KA, Southwick A, Tabor HK, Hartiala J, Allayee H, Grove ML, Tabibiazar R, Sidney S, Fortmann SP, Go A, Hlatky M, Iribarren C, Boerwinkle E, Myers R, Risch N, Quertermous T. Common polymorphisms of ALOX5 and ALOX5AP and risk of coronary artery disease. *Hum Genet.* 2008;123:399–408. <https://doi.org/10.1007/s00439-008-0489-5>.
  58. Pal K, Feng X, Steinke JW, Burdick MD, Shim YM, Sung SS, Gerald Teague W, Borish L. Leukotriene A4 hydrolase activation and leukotriene B4 production by eosinophils in severe asthma. *Am J Respir Cell Mol Biol.* 2019;60:413–9. <https://doi.org/10.1165/rcmb.2018-0175OC>.

**Publisher's Note** Springer Nature remains neutral with regard to jurisdictional claims in published maps and institutional affiliations.